Naval Research Laboratory

Washington, DC 20375-5320

NRL/MR/6360--19-9917

Synthesis, Characterization, and Testing of A12O3 Supported Tungsten Carbide as a Catalyst for the Reverse Water Gas Shift Reaction

James Morse
Heather D. Willauer

Materials and Systems Branch
Material Science and Technology Division

Jeffery W. Baldwin

Physical Acoustics Branch
Acoustics Division

Mitchell Juneau
Marc D. Porosoff

University of Rochester
Rochester, NY

December 16, 2019

REPORT DOCUMENTATION PAGE

Form Approved
OMB No. 0704-0188

1. REPORT DATE *(DD-MM-YYYY)*
16-12-2019

2. REPORT TYPE
NRL Memorandum Report

3. DATES COVERED *(From - To)*
08/07/2018 - 08/07/2019

4. TITLE AND SUBTITLE

Synthesis, Characterization, and Testing of A12O3 Supported Tungsten Carbide as a Catalyst for the Reverse Water Gas Shift Reaction

5a. CONTRACT NUMBER

5b. GRANT NUMBER

5c. PROGRAM ELEMENT NUMBER
NISE

6. AUTHOR(S)

James R. Morse, Heather D. Willauer, Jeffrey W. Baldwin, Mitchell Juneau,* and Marc D. Porosoff*

5d. PROJECT NUMBER

5e. TASK NUMBER

5f. WORK UNIT NUMBER
N2Q2

7. PERFORMING ORGANIZATION NAME(S) AND ADDRESS(ES)

Naval Research Laboratory
4555 Overlook Avenue, SW
Washington, DC 20375-5320

8. PERFORMING ORGANIZATION REPORT NUMBER

NRL/MR/6360--19-9917

9. SPONSORING / MONITORING AGENCY NAME(S) AND ADDRESS(ES)

Naval Research Laboratory
4555 Overlook Avenue, SW
Washington, DC 20375-5320

10. SPONSOR / MONITOR'S ACRONYM(S)

NRL-NISE

11. SPONSOR / MONITOR'S REPORT NUMBER(S)

12. DISTRIBUTION / AVAILABILITY STATEMENT

DISTRIBUTION STATEMENT A: Approved for public release; distribution is unlimited.

13. SUPPLEMENTARY NOTES

*University of Rochester, Department of Chemical Engineering, 500 Joseph C. Wilson Blvd, Rochester, NY 14627-0001
This work was performed by James Morse while under a Karles Fellowship

14. ABSTRACT

The conversion of CO2 to CO via the reverse water gas shift (RWGS) reaction is often envisioned as the first step in the large scale transformation of CO2 into value-added hydrocarbons. Accordingly, low cost and highly selective RWGS catalysts are desirable materials for sustainable CO2 utilization. Here, we describe synthesis, characterization, and performance evaluation of unpromoted, Na-promoted, and K-promoted tungsten carbide (WC) RWGS catalysts, supported on porous Al2O3. Scanning electron microscopy reveals significant differences in the distribution of the alkali-promoted WC catalysts, suggesting that the alkali metals serve as structural promoters, while X-ray photoelectron spectroscopy indicates slight differences in the electronic structure of the K-promoted WC. Performance data for the RWGS reaction at 300 and 350 °C shows all catalysts are active, with the alkali promoted catalysts demonstrating improved CO selectivity. Of the three catalysts, the highest CO yield is achieved using the K-promoted WC, demonstrating that K-WC can serve as a low cost, active, and selective RWGS catalyst. Additionally, we prepared and tested unpromoted W and W2C catalysts supported on Al2O3 to compare to the well characterized WC catalysts. These materials were also active for RWGS, but were less active and selective than the supported WC catalysts.

15. SUBJECT TERMS

Heterogeneous catalysis	Thermochemical catalysis	Reverse water gas shift
CO2 utilization	Tungsten carbide	Alkali

16. SECURITY CLASSIFICATION OF:			17. LIMITATION OF ABSTRACT	18. NUMBER OF PAGES	19a. NAME OF RESPONSIBLE PERSON
a. REPORT	**b. ABSTRACT**	**c. THIS PAGE**			James R. Morse
Unclassified Unlimited	Unclassified Unlimited	Unclassified Unlimited	Unclassified Unlimited	25	**19b. TELEPHONE NUMBER** *(include area code)* (202) 404-3418

Standard Form 298 (Rev. 8-98)
Prescribed by ANSI Std. Z39.18

This page intentionally left blank.

Contents

This page intentionally left blank.

Executive Summary:

The conversion of CO_2 to CO via the reverse water gas shift (RWGS) reaction is often envisioned as the first step in the large scale transformation of CO_2 into value added hydrocarbons. Accordingly, low cost and highly selective RWGS catalysts are desirable materials for sustainable CO_2 utilization. Here, we describe synthesis, characterization and performance evaluation of unpromoted, Na-promoted, and K-promoted tungsten carbide (WC) RWGS catalysts, supported on porous γ-Al_2O_3. Scanning electron microscopy reveals significant differences in the distribution of the alkali promoted WC catalysts, suggesting the alkali metals serve as structural promoters, while X-ray photoelectron spectroscopy indicates slight differences in the electronic structure of the K-promoted WC. Performance data for the RWGS reaction at 300 and 350 °C shows all catalysts are active, with the alkali promoted catalysts demonstrating improved CO selectivity. Of the three catalysts, the highest CO yield is achieved using the K-promoted WC, demonstrating K-WC can serve as a low cost, active and selective RWGS catalyst. Additionally, we prepared and tested unpromoted W and W_2C catalysts supported on γ-Al_2O_3 to compare to the well characterized WC catalysts. These materials were also active for RWGS, but were less active and selective than the supported WC catalysts.

This page intentionally left blank.

1.0 Background:

The depletion of fossil fuels and corresponding increases in atmospheric and oceanic CO_2 concentrations have motivated research in the field of alternative energy and inspired the development of technologies capable of sequestering and transforming CO_2 into fungible fuels. With CO_2 concentrations on the order of 100 mg L^{-1} (140 times greater than atmospheric levels),[1] the World's oceans offer a natural source of CO_2 which could be leveraged as a carbon feedstock. A recently patented process by the U.S. Navy realizes this concept, by demonstrating CO_2 and H_2 can be simultaneously extracted from seawater,[2–8] and subsequently used as reactants in the thermochemical hydrogenation of CO_2 into more valuable chemicals and fuels.[9–15]

The thermochemical hydrogenation of CO_2 to energy dense hydrocarbons can be achieved using a modified Fischer-Tropsch synthesis (FTS) process, by replacing CO with CO_2 (CO_2-FT). In a commonly proposed pathway, CO_2 is first converted to CO through the endothermic reverse water gas shift (RWGS) reaction, followed by hydrogenation of CO via exothermic FTS.[16–20] This process is often carried out using a single reactor system, allowing for simple reactor design and modularity. However, Typical FT temperatures range between 200-350 °C, while the RWGS reaction is equilibrium limited to 10-30% conversions in this same temperature range, at a 3:1 H_2:CO_2 ratio.[21] Accordingly, optimized CO_2-FT conditions have been challenging to establish.[17,18]

To increase the yield toward energy dense hydrocarbon products, it is ideal to operate RWGS at high conversions, while simultaneously minimizing CH_4 formation via the undesirable Sabatier reaction.[16,22,23] Although performing the RWGS at higher temperatures will undoubtedly improve CO yields, many RWGS catalysts exhibit decreased catalyst lifetimes at elevated temperatures. [24–26] Alternatively, we anticipate that at common FT temperatures, the impact of the thermodynamic limitations of RWGS can be minimized by (1) operating the process autothermally by recovering heat from the exothermic FT reaction, (2) by removing the produced water and subsequently recycling the reactor effluent to increase the CO2 conversion, and (3) by utilizing efficient and synergistic FT catalysts to rapidly consume intermediate CO, further driving RWGS. [17,18,27] Accordingly RWGS catalysts witch can effectively function under common FTS conditions represent an important class of materials.

Platinum catalysts dispersed on metal oxide supports have shown reasonable activity and selectivity for the RWGS reaction at relatively low temperatures (300 °C),[28–30] but the cost of these catalysts make them non-ideal for practical applications. Transition metal carbides (TMCs) have received significant attention as alternatives to precious metal catalysts for their comparable catalytic activities for various reactions,[31–33] including RWGS.[34] The addition of promoting species to TMCs can further improve performance by attenuating the structural and electronic properties of the catalyst.[35] In particular, alkali promoters reduce CH_4 selectivity in TMCs,[36,37] and recent studies by our group demonstrate the selectivity towards CO increases from ~75% to 95% for the low temperature RWGS reaction when potassium is incorporated into a Mo_2C-based catalyst.[38] These findings indicate that promoted TMCs are selective and low-cost alternative catalysts for the low temperature RWGS reaction.

Of the TMC family, WC is frequently compared to Mo_2C in terms of catalytic properties, with similar activities observed for deoxygenation,[39] hydrogenation[40–42] and reforming reactions.[43–45] A recent comparison of the RWGS activity of various bulk TMC catalysts demonstrates oxygen binding energy is a descriptor of activity, with WC and Mo_2C exhibiting the highest CO_2 conversions.[34] These trends suggest

---

Manuscript approved September 5, 2019.

WC can be optimized to function as an effective low-temperature RWGS catalyst, similar to Mo_2C.[38] However, WC has not yet been further investigated as a catalyst for the RWGS reaction.

In this manuscript, we describe the synthesis and testing of unpromoted and alkali metal promoted WC supported on high surface area γ-Al_2O_3 (WC/γ-Al_2O_3) as low-cost and selective catalysts for the RWGS reaction. Characterization with X-ray diffraction (XRD), pulsed chemisorption, N_2 physisorption, scanning electron microscopy (SEM) and X-ray photoelectron spectroscopy (XPS) demonstrate that alkali metals act as structural and electronic promoters, attenuating surface chemistry, altering catalyst dispersion and slightly reducing the oxidation state of the active WC component. Additionally, we describe the synthesis and testing of W_2C/γ-Al_2O_3 and W/γ-Al_2O_3 catalysts for the RWGS, however, detailed characterization and discussion of these systems are limited, as they were found to be less active for the RWGS. Reactor studies indicate that the alkali metals increase CO selectivity for the WC/γ-Al_2O_3 catalysts, with the K promoter exhibiting the highest increase in overall CO yield. This study extends the library of low-cost, low-temperature RWGS catalysts, and further demonstrates that alkali promoters are an effective means to tune RWGS selectivity.

2.0 Objective:

The objective of this work is to enable the development of efficient, stable, and affordable catalyst systems capable of thermochemically reducing carbon dioxide into fungible chemicals and fuels. To accomplish this objective, we synthesize, characterize, and then test various tungsten based catalyst systems under relevant working conditions to identify and optimize the catalytic activity of these materials for the reverse water gas shift reaction, an important first step in the utilization of carbon dioxide.

3.0 Experimental:

3.1 Materials:

Ammonium metatungstate hydrate ($(NH_4)_6H_2W_{12}O_{40} \cdot xH_2O$) 99.99% trace metals basis, sodium carbonate (Na_2CO_3) >99%, and potassium carbonate (K_2CO_3) >99% were purchased from Sigma Aldrich. γ-Al_2O_3 powder (>97%) was purchased from STREM Chemicals. All gases used for catalyst synthesis and testing were supplied from Earlbeck Gases & Technologies, while the gases used for pulse chemisorption were of research grade purity and purchased from Airgas.

3.2 Catalyst Preparation:

The WC/γ-Al_2O_3 catalysts were synthesized by the evaporation deposition method. Briefly, 20.2 g ammonium metatungstate hydrate was dissolved in 300 mL deionized water using a magnetic stir bar. Five minutes later, 30.0 g γ-Al_2O_3 powder was mixed into the solution. The excess water was evaporated over the course of 72 hours under gentle stirring at 60 °C. For the Na and K promoted catalysts, identical procedures were followed, however, 1.14 g of Na_2CO_3 or 1.48 g of K_2CO_3 were added with the tungsten precursor. These precursor amounts correspond to 1:4:15 X/W/γ-Al_2O_3 molar ratios (X= K, or Na), which are commensurate to the ratios described for our previously reported K-Mo_2C/γ-Al_2O_3 catalyst.[38]

Once dry, the impregnated supports were gently ground with a mortar and pestle, and then calcined at 600 °C for 12 hours. The catalysts were pelletized under a force of 1 ton for 10 minutes, then gently ground and sieved to a particle size of 200-350 µm prior to carburization to improve mass transfer. 5 g of each catalyst was then individually carburized under a 20% CH_4/H_2 blend at 300 mL min^{-1} for 20 hours at 825 °C. The catalysts were then cooled to room temperature under the carburizing atmosphere and finally passivated with a 1% O_2/N_2 blend at 10 mL min^{-1} overnight. After passivation, the catalysts were exposed to ambient atmosphere and a portion of each carburized catalyst was saved for analysis and future testing. These samples are subsequently referred to as *"as synthesized".*

$W_2C/\gamma\text{-}Al_2O_3$ and $W/\gamma\text{-}Al_2O_3$ catalysts were generated using the same calcined and pelletized $W\text{-}Al_2O_3$ precursor described above, but reduced under different conditions. To generate the W_2C phase, the calcined material was carburized under a 20% CH_4/H_2 blend at 300 mL min^{-1} for 20 h at 550 °C. The material was then cooled to room temperature and passivated with a 1% O_2/N_2 blend at 10 mL min^{-1} overnight. To generate the W phase, the calcined material was reduced under flowing H_2 gas at 300 mL min^{-1} for 20 hours at 700 °C, then cooled to room temperature and passivated as described above.

3.3 Removal of Polymeric Carbon:

To remove polymeric carbon deposited during the carburization step, the $WC/\gamma\text{-}Al_2O_3$ catalysts were reduced under an H_2 atmosphere using a slightly modified version of a previously published procedure.[46] Briefly, the carburized catalysts were heated to 750 °C under H_2 at a flow rate of 100 mL min^{-1} for 3.5 hours. The reduction of polymeric carbon was characterized by the evolution of CH_4 using gas chromatography. Following this, H_2 flow was cut off, a flow of He gas was introduced at 100 mL min^{-1}, and the catalysts were heated to 800 °C for 0.5 hours to promote equilibration of the bulk and surface compositions. Once cooled to room temperature, the catalysts were again passivated with a 1% O_2/N_2 blend overnight. These samples are subsequently referred to as *"H_2 treated"*. This procedure was not performed for the $W_2C/\gamma\text{-}Al_2O_3$ and $W/\gamma\text{-}Al_2O_3$ catalysts.

3.4 Temperature Programmed Carburization (TPC):

TPC was performed using a Micromeritics AutoChem II to qualitatively compare the consumption of H_2 and CH_4 under carburization conditions. Under a 20% CH_4/H_2 blend flowing at 50 mL min^{-1}, 100 mg of the $WO_3/\gamma\text{-}Al_2O_3$ precursor was heated to 950 °C at a ramp rate of 10 °C min^{-1}. The effluent gases were measured as a function of temperature via an in-line thermal conductivity detector (TCD).

3.5 X-Ray Diffraction (XRD):

Measurements were performed on a Rigaku Smartlab X-ray diffractometer using Cu Kα monochromatized radiation operated at 44 kV and 40 mA at room temperature over the range of 20-90° 2θ. X-ray diffraction patterns for the catalysts were referenced to reported patterns from multiple databases.

3.6 Pulse Chemisorption:

All pulse chemisorption experiments were performed at 30 °C using a Micromeritics AutoChem II. Prior to each measurement, the catalyst was reduced in H_2 for 2 hours at 350 °C. The analysis gas was then pulsed over the catalyst ten times, or until the amount of analyte adsorbed by the catalyst was equal to zero. Because pure CO_2 was used for the pulse CO_2 adsorption experiments, CO_2 was only pulsed over the catalyst five times. Pulse chemisorption experiments were performed for CO, CO_2 and H_2 to determine the catalytically active surface area with respect to each adsorbate. The concentration of the active gases were 5% CO in He, 100% CO_2 and 10% H_2 in Ar, and were certified mixtures and/or research grade gases obtained from Airgas.

3.7 BET Surface Area Analysis:

Nitrogen adsorption analysis was performed at -196 °C, using a Beckman-Coulter S.A. 3100 Surface Area Analyzer. Prior to the measurement, the catalyst was degassed at 300 °C for 60 min under 4 µm Hg vacuum. To account for any temperature induced changes to the catalyst support, the bare γ-Al_2O_3 was calcined, pelletized and heated under the same carburizing atmosphere as the WC catalysts before BET characterization.

3.8 Scanning Electron Microscopy (SEM):

SEM characterization was performed using a Carl Zeiss Supra 55 Schottky thermal field-emitting microscope with a 30 µm aperture 10 kV accelerating voltage. For EDS measurements, an Oxford Instruments X-Max was inserted into the SEM chamber using an accelerating voltage of 5 kV and working distance of 8.5 mm.

During the SEM measurements, many granules of the supported catalyst were surveyed, and no significantly different structures or elemental distributions were observed other than what is presented in this manuscript.

3.9 X-ray Photoelectron Spectroscopy (XPS):

Measurements were performed over the *"as synthesized"* and *"H_2 treated"* WC/γ-Al_2O_3 catalysts using a commercial XPS system (Thermo Scientific Kα) equipped with a monochromatic $Al_{K\alpha}$ source and an 1808 double focusing hemispherical analyzer with 128-channel detector. The nominal XPS spot size was 400 mm^2. Settings for data collection were: Pass Energy=20 eV, dwell time=100 ms, energy step size=0.15 eV over 40 averaged scans. Charge compensation was necessary. Calibration of the instrument was confirmed using the C1s peak of a bare γ-Al_2O_3 powder at 284.8 eV.

3.10 Reactor studies:

For a typical experiment, 1 g of catalyst pellets were loaded into a 0.25 in stainless-steel reactor. The catalyst bed was reduced under H_2 at 350 °C and 0.5 MPa at a flow rate of 50 mL min^{-1} for a total of 2.5 hours. The catalyst bed was then isolated as the rest of the reactor system was pressurized to 2.0 MPa with a blend of N_2, CO_2 and H_2 gases at ratios commensurate with the subsequent experimental flowrates. Once pressurized, the reactant gases were introduced to the catalyst bed at a 3:1 H_2/CO_2 ratio, with flowrates corresponding to the reported weight hourly space velocities (WHSV). N_2 was used as an internal standard to quantify CO_2 conversion and CO yield. Reactant flowrates were controlled using programmable mass flow controllers (Brooks SLA5850). Reactions were run for 16 hours and monitored by gas chromatography to ensure a steady state had been achieved. Unless otherwise noted, all reported catalytic data refers to the experiments after 16 hours on stream. To prevent deterioration of the GC columns by water, all effluent reaction gas was passed through a cold trap (5 °C) before characterization by gas chromatography (Agilent 7890A).

4.0 Results and Discussion:

4.1 Catalyst Synthesis and Characterization:

Temperature programmed carburization (TPC) of metal oxide precursors using a flowing blend of H_2 and CH_4 is a common method to obtain supported carbide catalysts.[40,44,47–49] It is generally agreed that the carburization of WO_3 occurs as a multi-step process involving reduction of tungsten oxide species to metallic tungsten, followed by carburization.[50–52] The exact temperatures of these transitions depend on both precursor-support interactions, as well as the presence of a promoting species.[52–54] In order to determine the effect of the alkali promoters on the carburization of WO_3 supported on γ-Al_2O_3, as well as the optimal synthesis conditions for the WC catalyst samples, a series of TPC experiments were carried out. Figure 1 displays the response of the TCD detector used to measure the composition of the effluent gas during the TPC experiments.

From a qualitative viewpoint, increases to the TCD signal relative to the baseline correlate to a decrease in the overall H_2:CO_2 ratio of the effluent gas, which can be considered to correspond to a greater rate of H_2 consumption relative to CH_4. Conversely, decreases to the TCD signal can be considered to correspond to a greater rate of CH_4 consumption. Although the TPC curves in Figure 1 exhibit the same characteristic peaks for the three precursors, differences in the shapes and position of the peaks demonstrate the effects of Na and K-promotion on the carburization of WO_3 supported on γ-Al_2O_3. Peaks **A** and **B**, located between 500-750 °C, likely correspond to the reduction of the supported WO_3 precursor to WO_2 and W, respectively. These peaks are shifted to higher temperatures for both the Na and K-promoted catalysts, indicating the alkali promoters inhibit the reduction of the metal oxide precursors, which is in agreement with previous studies.[55,56]

More notably, the inverse peak **C**, associated with the complete carburization of the precursors to WC, is shifted to lower temperatures for the Na and K-promoted catalysts, indicating the rate of carburization increases in the presence of alkali promoters. Further decreases to the TCD signal after complete carburization most likely correspond to the catalyzed decomposition of CH_4 onto the WC surface in the form of polymeric carbon. These TPC data were subsequently used as a guide to controllably synthesize supported WC catalysts via temperature programmed carburization. In addition, unpromoted W and W_2C catalysts supported on γ-Al_2O_3 were also synthesized, in order to study the catalytic activity of other tungsten phases for the RWGS (see the Experimental Section for synthetic details).

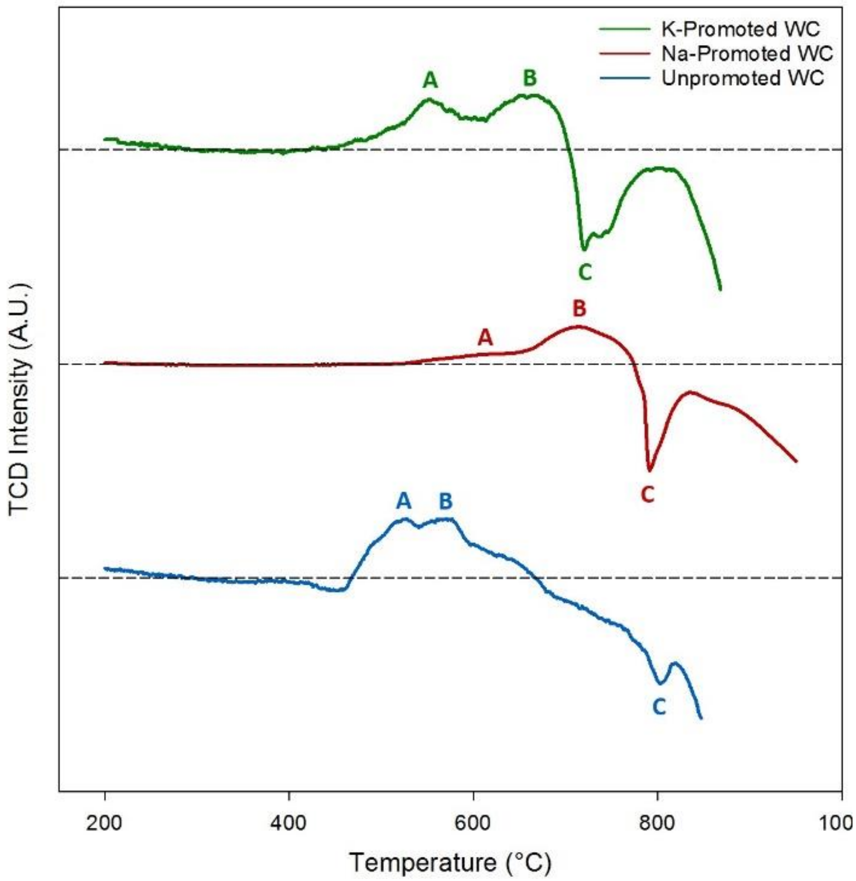

Figure 1: Temperature programmed carburization for unpromoted (blue), Na-promoted (red), and K-promoted (green) tungsten catalyst precursors. Points A and B represent reduction of tungsten oxides, while point C represents complete carburization.

XRD patterns for the three *"as synthesized"* WC catalysts, along with a reference pattern for the γ-Al_2O_3 support are shown in Figure 2a, while the unpromoted W and W_2C samples are provided in figure 2b. Figure 2a demonstrates that all three WC patterns are nearly identical, with clear reflections corresponding to the hexagonal WC phase present in each sample. Much weaker reflections corresponding to the cubic WC_{1-x} phase are also present for each of the characterized samples, with the unpromoted catalyst exhibiting the strongest reflections. This carbon deficient phase has been observed previously in the temperature programmed carburization of tungsten species, and is believed to be a meta-stable intermediate resulting from incomplete carburization.[57,58] The observation that this phase constitutes a greater fraction of the unpromoted sample is in line with the TPC experiments, suggesting alkali promoters facilitate tungsten carburization. Figure 2b clearly demonstrates that the W_2C and W phases can also be accessed by slightly altering the conditions of the carburization step.

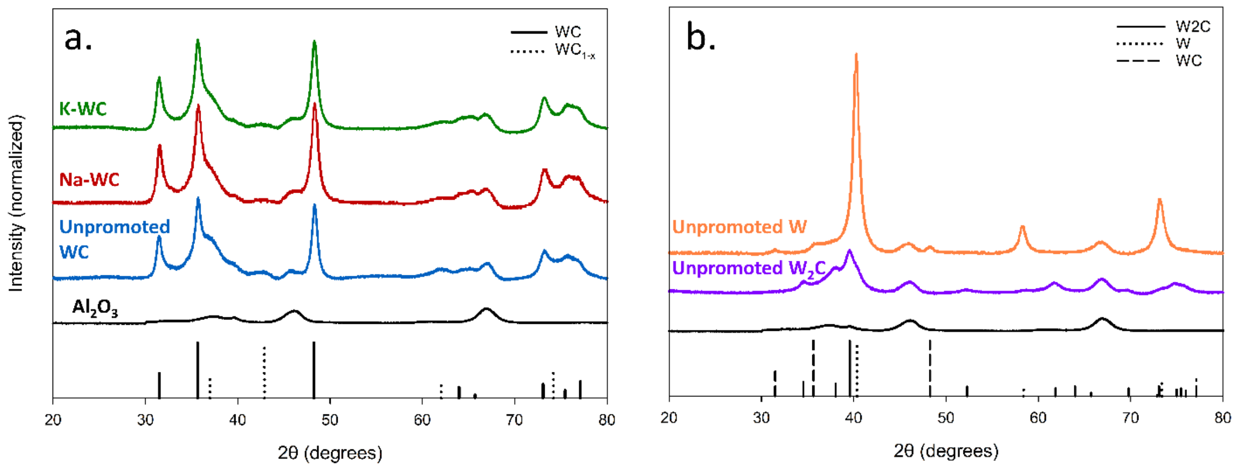

Figure 2: X-ray diffraction patterns corresponding to a) the "as synthesized" unpromoted (blue), Na-promoted (red), and K-promoted (green) WC/γ-Al_2O_3, and b) unpromoted W_2C/γ-Al_2O_3 (purple) and unpromoted W/γ-Al_2O_3. Reference patterns corresponding to the appropriate crystal structures are also included, along with patterns for the bare γ-Al_2O_3 support.

As demonstrated in Figure 1, as well as by previous authors, the high temperatures required to carburize WO_3 to WC can also cause deposition of polymeric carbon onto the carbide surface, blocking catalytically active sites.$^{46,57,59–61}$ For this reason, freshly synthesized WC catalysts are often treated under flowing H_2 at elevated temperatures to remove the unwanted surface carbon in the form of CH_4.^{46,49,59,61,62} The duration and temperatures at which the WC is exposed to H_2 treatments must be carefully chosen, however, as prolonged exposure to H_2 can lead to reduction of the WC to metallic W.^{46,49,62} Rebeiro et al. have demonstrated that for the removal of surface polymeric carbon from WC, the maximum rate of CH_4 generation correlates with the nearly complete removal of surface polymeric carbon, and that H_2 treatments much beyond this can lead to the reduction of WC to metallic W.^{46} Accordingly, portions of the as synthesized WC catalyst samples were treated with H_2 at elevated temperatures to remove polymeric carbon, which was characterized in real time using gas chromatography. Figure 3a shows the evolution of CH_4 from the three WC/ γ-Al_2O_3 samples when treated under flowing H_2 for 3.5 h at 700 °C, while Figure 3b shows the evolution of CH_4 from the Na and K-promoted samples under H_2 at 750 °C. Peak CH_4 evolution is observed for the unpromoted WC sample when treated with H_2 at 700 °C within the time frame tested, whereas longer times or higher temperatures are required to remove appreciable amounts of polymeric carbon from the Na and K-promoted WC samples. It is only when heated under H_2 at 750 °C, is peak CH_4 evolution is observed for the Na and K-promoted WC samples at rates comparable to that of the unpromoted WC at 700 °C. We speculate these trends may be due greater quantities of polymeric carbon on the Na and K-promoted WC samples. It is possible the increased rates of carbide formation due to the presence of alkali promoters would also increase the rate of carbon deposition. Additionally, it's probable these thicker carbon layers, not in direct contact with the catalytically active WC surface, are not as readily reduced and therefore would be removed at slower rates.

To understand the effect of polymeric carbon on the catalytic activity of the WC/γ-Al_2O_3, a portion of all three of the *"as synthesized"* WC catalysts were saved for future testing. The rest of the WC catalyst samplers were treated with H_2 at 750 °C for 3.5 h. These are subsequently referred to as *"H_2 treated"*. The *"as synthesized"* catalysts were found to exhibit identical X-ray diffraction patterns to the corresponding *"H_2 treated"* catalysts (not shown), indicating these H_2 treatments did not alter the bulk crystal structure.

It should be noted that this H_2 treatment was not performed for either the W or W_2C catalysts, as these samples were not exposed to high enough temperatures to induce polymeric carbon deposition.

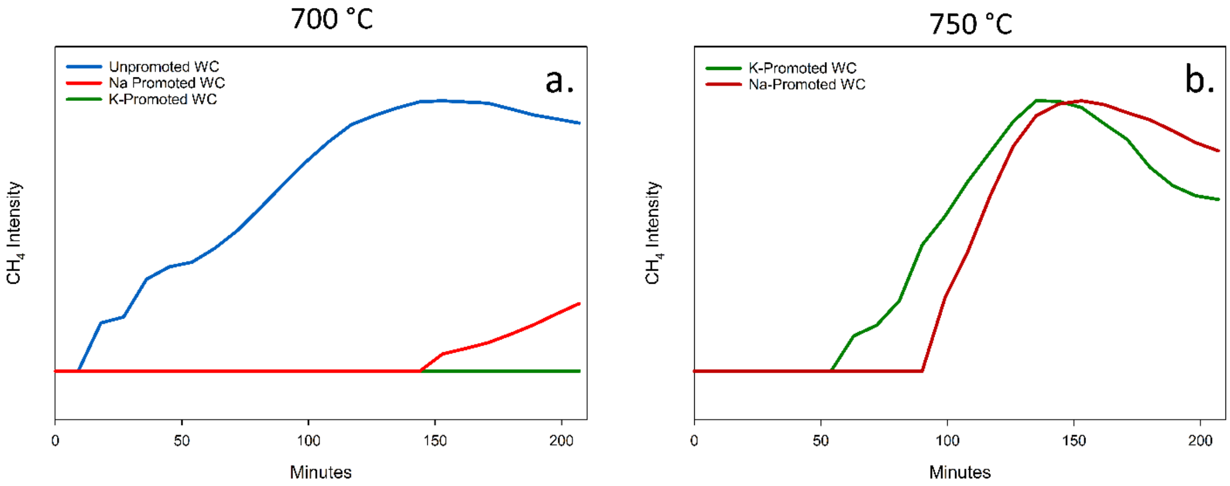

Figure 3: Normalized TCD signal corresponding to evolved CH_4 gas during H_2 treatments for the WC/γ-Al_2O_3 catalysts at a) 700 °C and b) 750 °C.

To directly visualize the distribution of the tungsten species across the γ-Al_2O_3 support, scanning electron microscopy coupled with energy dispersive X-ray spectroscopy (SEM-EDS) was carried out on the three *"H_2 treated"* WC catalysts. For each sample, multiple micrographs were collected at various positions across the catalysts. Figure 4 displays SEM-EDS images that can be considered representative for the three WC catalyst samples (additional SEM-EDS images are provided in the Supplemental Information). The unpromoted WC/γ-Al_2O_3 consists of localized tungsten distributions on the order of 1 µm in diameter, and clear segregation between the tungsten species and γ-Al_2O_3 support can be observed. On the other hand, the Na and K-promoted catalysts are composed of much smaller, better dispersed tungsten species, which appear to be localized to domains on the order ~50-200 nm. While discrete nanoscale WC particles may exist below the spatial resolution of SEM, these data demonstrate clear structural differences amongst the catalyst samples, indicating Na and K serve as structural promoters in the synthesis of WC/γ-Al_2O_3.

Further evidence of the structural effect of alkali promoters are shown by the BET data in Table 1. As shown in the table, the surface area of the porous γ-Al_2O_3 support is 160 m^2 g^{-1}, which is greater than any of the WC/γ-Al_2O_3 catalysts. Of the three catalyst systems, the unpromoted WC/γ-Al_2O_3 has the greatest surface area. Both the Na and K-promoted WC exhibit significantly lower surface areas, which we suggest is due to blockage of the γ-Al_2O_3 micropores due to the better dispersion of the alkali promoted species across the high surface area support.[63,64] An increase in surface area is observed after the unpromoted catalyst is treated with H_2, which we believe is caused by the removal of polymeric surface carbon. Interestingly, however, very little change in the surface areas of the alkali promoted catalysts are observed following hydrogen treatment.

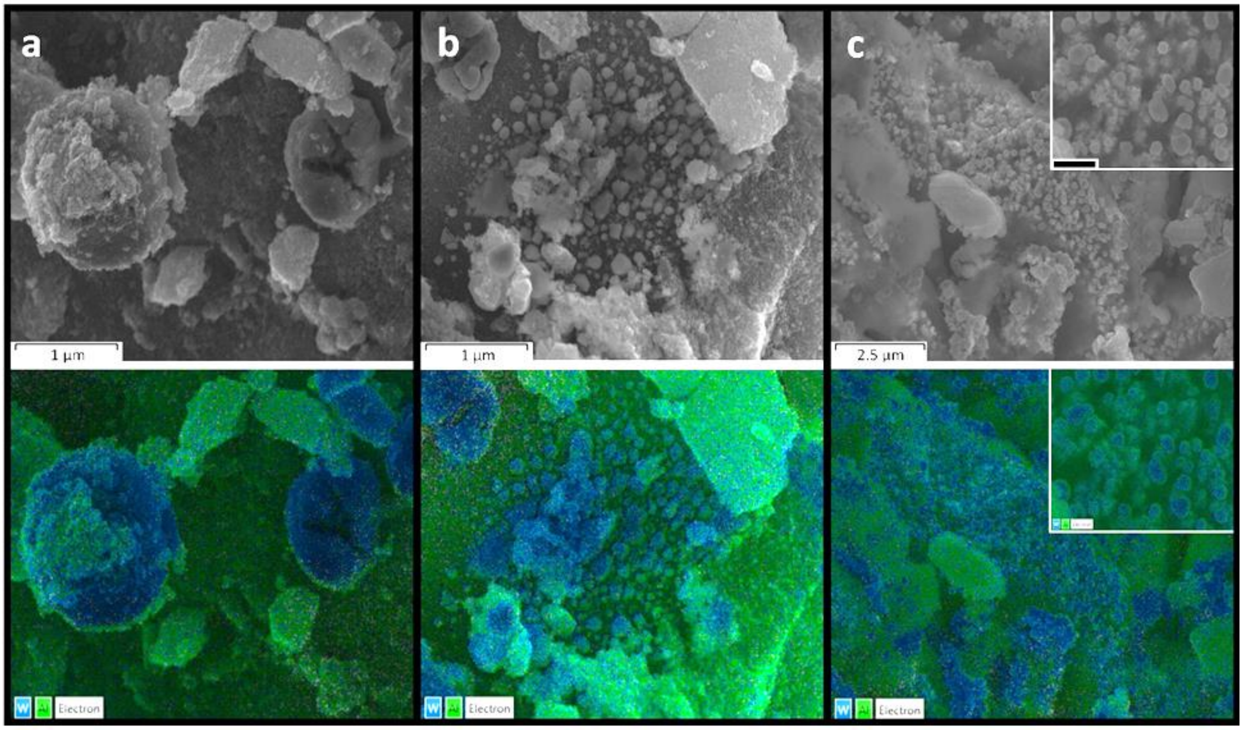

Figure 4: SEM images and corresponding EDS maps for the "H_2 treated" a) unpromoted, b) Na-promoted, and c) K-promoted WC/γ-Al_2O_3. Scale bar in the inset of image c) corresponds to 500 nm. EDS signals corresponding to W are in blue, while signals corresponding to Al are mapped in green.

Table 1: Calculated Crystallite Size and BET Surface Area for WC/ γ-Al_2O_3 Catalysts

	WC Crystallite Size (nm)[a]	BET Surface Area ($m^2 g^{-1}$)
γ-Al_2O_3	N.A.	160
"As Synthesized" γ-Al_2O_3 – Unpromoted WC	12	122
"H_2 Treated" γ-Al_2O_3 – Unpromoted WC	12	136
"As Synthesized" γ-Al_2O_3 – Na-WC	11	93
"H_2 Treated" γ-Al_2O_3 – Na-WC	11	97
"As Synthesized" γ-Al_2O_3 – K- WC	11	83
"H_2 Treated" γ-Al_2O_3 – K- WC	11	85

[a] *Crystal size estimated using the Scherrer formula.*

In addition to structural effects, previous authors have directly observed electronic promotion via alkali metals, which strengthen CO and CO_2 adsorption, while weakening H_2 adsorption. Addition of alkali metals is therefore hypothesized to result in a lower H_2/CO_x ratio on the catalyst surface, thus inhibiting hydrogenation activity, and reducing the generation of CH_4.[55,63,65,66] To compare the adsorption of the relevant chemical species for the RWGS reaction, CO, CO_2, and H_2 uptake experiments on the three *"H_2 treated"* WC-based catalysts are shown in Table 2. CO adsorption is about an order of magnitude greater for the Na-WC/γ-Al_2O_3 sample relative to the K-promoted and unpromoted WC/γ-Al_2O_3 samples, while the CO_2 uptake experiments demonstrate both Na and K-promoted samples adsorb significantly more CO_2 than the unpromoted catalyst. The H_2 uptake data, however, are of comparable magnitude for all three samples. Taken together, these data suggest a shift to lower H_2/CO_2 ratios on the surface of the alkali promoted catalysts, relative to the unpromoted WC/γ-Al_2O_3, which we hypothesize promotes improved CO selectivity for the RWGS reaction.

Table 2: CO, CO_2 and H_2 Uptake for WC/γ-Al_2O_3 Catalysts.

	CO uptake (cm^3/g)	CO_2 Uptake (cm^3/g)	H_2 Uptake (cm^3/g)
Unpromoted-WC *“H_2 Treated”*	0.0243	0.0862	4.78
K-WC *"H_2 Treated"*	0.0478	0.488	7.27
Na-WC *"H_2 Treated"*	0.366	1.79	4.54

The promotional effects of the alkali species on WC are further characterized by the surface sensitive XPS measurements in Figure 5. Figure 5a shows the XPS signals corresponding to the W4f region for the three *“as synthesized”* WC catalysts, while Figure 5b shows the same data set for the *“H_2 treated”* catalysts. Prior to H_2 treatment, all catalysts display a single pair of peaks, corresponding to the $W4f_{7/2}$ and $W4f_{5/2}$ signatures of WC, respectively.[61,67] After H_2 treatment, the same carbide signatures are present, along with newly developed shoulders at slightly higher binding energies, representative of tungsten oxide species.[67] The fact that these oxide species are not observed in the *“as synthesized”* catalysts indicates polymeric surface carbon deposited during the synthesis of the catalysts is significant enough to envelop the catalyst surface, preventing oxidation. These results are in agreement with the data described in Figure 3, and confirm that the H_2 treatment removes the polymeric carbon from the catalyst, allowing the catalyst surface to be exposed and subsequently oxidized during passivation.

Additionally, as shown in Figure 5, the W4f binding energy for the K-promoted WC/γ-Al_2O_3 is about 0.2 eV lower than the unpromoted and Na-promoted catalysts for both the *“as synthesized”* and *“H_2 treated”* WC catalysts. This indicates the K-promoted WC/γ-Al_2O_3 exists in a slightly more reduced state than the other two WC-based catalysts, providing further evidence that potassium also acts as an electronic promoter. These results correlate well with previous studies, which report potassium serves as an electronic promoter for transition metal catalysts, reducing the oxidation state and altering the catalytic activity.[68–70]

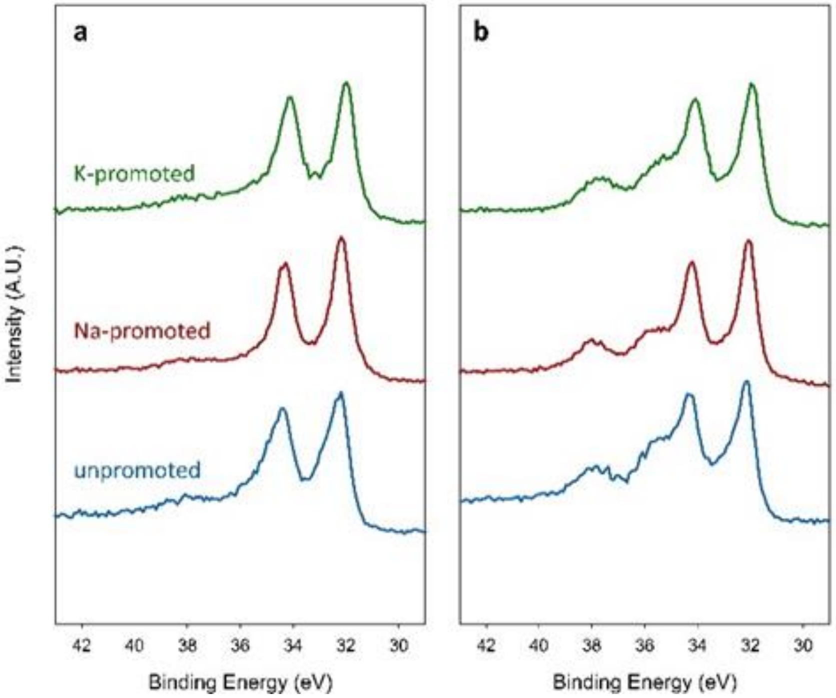

Figure 5: XPS spectra of the W4f region for unpromoted, Na-promoted, and K-promoted WC/γ-Al_2O_3 a) "as synthesized" and b) "H_2 treated".

4.2 RWGS Performance:

The activity and selectivity for the three *"as synthesized"* and *"H_2 treated"* WC/γ-Al_2O_3 catalysts were tested for the RWGS at 300 and 350 °C, respectively, using a weight hourly space velocity (WHSV) of 1.01 mL g^{-1} s^{-1} and a H_2:CO_2 ratio of 3:1 at a pressure of 2.0 MPa. For comparison, the unpromoted W_2C/γ-Al_2O_3 and W/γ-Al_2O_3 catalysts were also tested under these conditions. The results are tabulated in Table 3, along with our previously reported data for the Mo_2C/γ-Al_2O_3 catalyst. From these data, it is clear various tungsten materials are active for the RWGS reaction, however, appreciable activity is only observed for the *"H_2 treated"* WC catalysts.

At 300 °C, the CO_2 conversion for all of the W-based catalysts are lower compared to the previously reported Mo_2C catalyst, which was tested under identical conditions.[38] However, when the reaction temperature is increased to 350 °C, a substantial increase in activity is observed, and the CO_2 conversion over the WC-based catalysts reaches 13 to 24%. Previous studies comparing Mo_2C and WC catalysts have also noted greater activity for the Mo_2C systems under equivalent conditions.[39,40,45] This is typically attributed to the increased surface area of Mo_2C, as the higher carburization temperatures required to synthesize the WC phase may cause sintering of the WC domains, thereby lowering the catalytic activity.[39,45] Although such sintering may be partially responsible for the lower CO_2 conversions observed in this work, it is also possible Mo_2C is intrinsically more active than WC for the RWGS reaction. At 350 °C, the other tungsten phases (W and W_2C) also demonstrate improved RWGS activity, but at lower overall conversions, demonstrating the thermodynamically stable WC to be the most efficient W-phase under these conditions.

To characterize the intrinsic activity of the WC catalysts, apparent activation energies for the *"H_2 treated"* catalysts using Arrhenius plots are provided in Figure 6. These values are also included in Table 3, along with the apparent activation energies previously reported for the Mo_2C-based catalyst. The supported WC catalysts do indeed possess higher activation energies, between 14.9 and 17.7 Kcal mol^{-1}, than those reported for the Mo_2C catalysts, which are between 11.4 and 14.0 Kcal mol^{-1}. The calculated activation energies for the Na and K-promoted WC/γ-Al_2O_3 are also lower than the unpromoted WC/γ-Al_2O_3 catalyst, which is in agreement with the previously observed trends for the Mo_2C-based RWGS catalysts.[38]

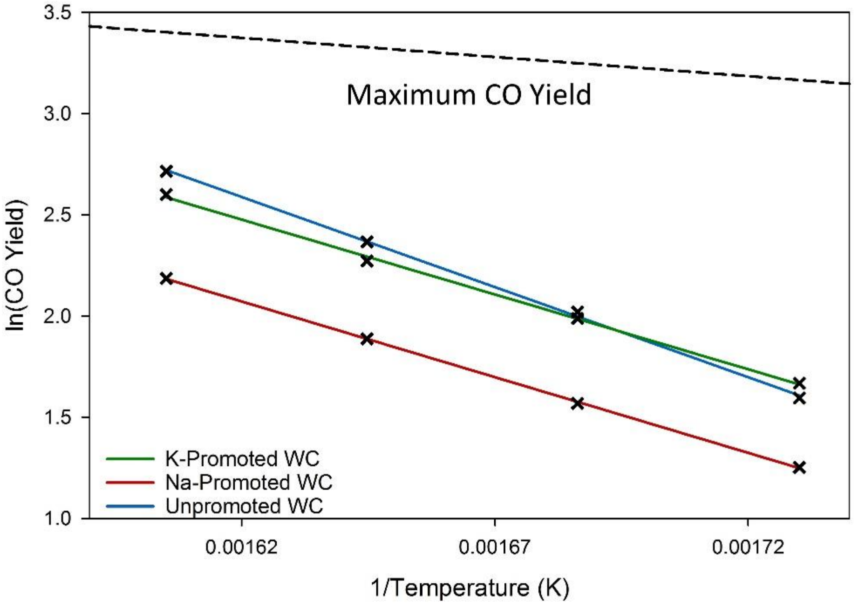

Figure 6: Arrhenius plots for "H_2 treated" unpromoted (blue), Na-promoted (red), and K- promoted (green) WC/γ-Al_2O_3The dotted line corresponds to the thermodynamic maximum CO yield under the conditions tested.

With the Na and K-promoted WC catalysts exhibiting lower activation energies and better overall dispersion relative to the unpromoted WC catalyst, it might be anticipated that the alkali-promoted WC catalysts would exhibit greater activity. Under the conditions described for Table 3, however, CO_2 conversions at 350 °C for the *"H_2 treated"* Na and K-promoted catalysts are 13.6 and 20.3%, respectively, while the unpromoted *"H_2 treated"* catalyst achieves a CO_2 conversion of 24.3%. A similar decrease in RWGS activity was observed with the addition of K to Mo_2C in our previous work,[38] and various other authors have also described decreases in carbide activity due to the addition of alkali promoters for other catalytic reactions.[69,71,72]

Such changes to catalyst performance may be rationalized by structural and electronic effects from addition of alkali metal promoters. For example, structural promoters may alter the geometry and crystallographic orientation of the catalyst, which in turn can affect the availability and activity of surface sites.[73] These structural changes are observed for the WC-based catalysts upon alkali metal addition via lower BET surface areas, altered tungsten dispersion, and decreased WC_{1-x} content. Electronic promotion, on the other hand, can result in attenuated adsorption and disassociation of reactants and intermediates, thus affecting catalytic activity and selectivity.

Electronic effects are primarily observed over the WC catalysts via the shift of the W4f XPS spectrum to a more reduced state upon the addition of potassium. It is also notable that the Na-promoted WC demonstrates the highest CO_2 and CO uptakes in Table 2 as well as the lowest CO yields under all of the conditions tested, suggesting increased CO_2 and CO binding energies. These electronic promotional effects are also consistent with previous studies by the group over K-Mo_2C.[38,74] Although it may be difficult to precisely decouple the structural and electronic effects of promoters in the current study, the addition of alkali metal promoters to WC/γ-Al_2O_3 clearly results in increased CO selectivity.

Table 3: Comparison of catalyst activity, selectivity and experimentally determined activation energies. Conversion and selectivity values reported for tungsten based catalysts were collected after 16 hours on stream, using a 3:1 H_2/CO_2 ratio at a WHSV of 1.01 mL $g^{-1}s^{-1}$ and a total pressure of 2.0 MPa.

	300 °C		350 °C		
	CO_2 Conversion (%)	CO Selectivity (%)	CO_2 Conversion (%)	CO Selectivity (%)	E_A (Kcal mol^{-1})*
Mo_2C[38]	19.9	73.5	N.A.	N.A.	14.0
2 wt% K-Mo_2C[38]	18.1	95.9	N.A.	N.A.	11.4
Unpromoted-WC *"as synthesized"*	3.8	90.0	14.0	96.4	N.A.
K-WC *"as synthesized"*	1.4	100	5.3	100	N.A.
Na-WC *"as synthesized"*	1.7	100	3.7	100	N.A.
Unpromoted WC *"H_2 Treated"*	8.8	89.9	24.3	88.0	17.7
K-WC *"H_2 Treated"*	4.8	100	20.3	98.1	15.0
Na-WC *"H_2 Treated"*	1.9	100	13.6	100	14.9
W_2C/γ-Al_2O_3	10.3	80.6	22.7	82.6	N.A.
W/γ-Al_2O_3	5.0	100	15.6	95.7	N.A.

**Activation energies were determined experimentally using Arrhenius plots.*

To test if the CO selectivities of the alkali promoted catalysts could be maintained at greater CO_2 conversions, the catalysts were tested at 350 °C under identical conditions to those described for Table 3, but at various reactant flow rates. Figure 7a plots the CO selectivity as a function of CO_2 conversion for the three *"H_2 treated"* catalysts at varying WHSVs, while Figure 7b plots the CO yield (CO selectivity times conversion) as a function of reactant flow rate for the same data set. For reference, the CO yield corresponding to the thermodynamic maximum of the RWGS at this temperature is indicated as a dashed line in Figure 7b.

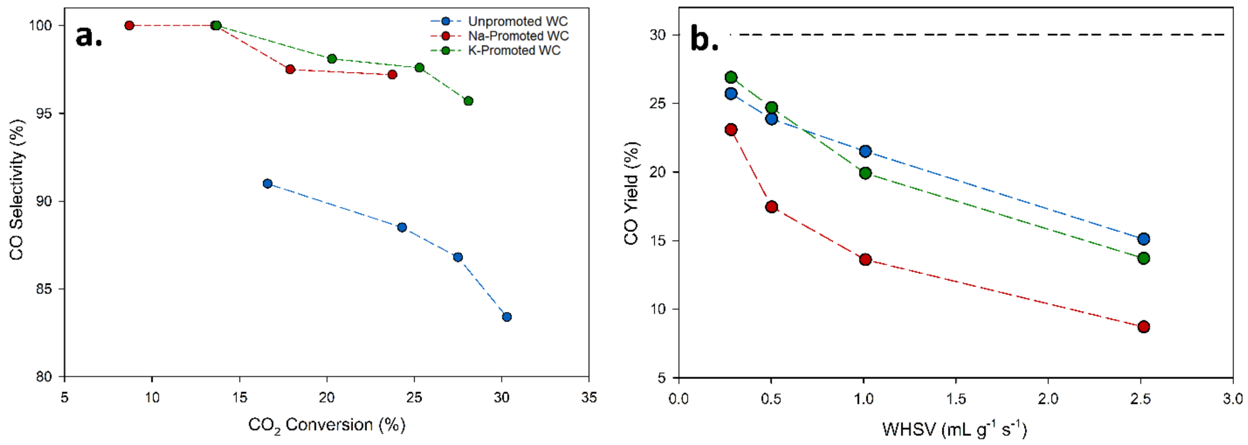

Figure 7: a) CO selectivity as a function of CO2 conversion at 350 °C for "H_2 treated" unpromoted (blue), Na-promoted (red), and K-promoted (green) WC/γ-Al_2O_3. b) CO yield at 350 °C as a function of WHSV for "H_2 treated" unpromoted (blue), Na-promoted (red), and K-promoted (green) WC/γ-Al_2O_3. Tests were performed at 350 °C using varying WHSVs and a 3:1 H_2:CO_2 ratio at a total pressure of 2.0 MPa.

When the WHSV is lowered to 0.50 mL g^{-1} s^{-1}, CO_2 conversions for the Na and K-promoted catalysts are increased to 17.9 and 25.3 %, respectively, yet they still exhibit CO selectivities > 95 %, demonstrating that even at similar CO_2 conversions, CO selectivities are greater for the alkali promoted catalysts. As displayed in Figure 7b, maintaining such high selectivities under the greater CO_2 conversions is especially notable for the K-promoted catalyst, which displays the greatest CO yields of the three catalysts when WHSVs are lowered to 0.50 mL g^{-1} s^{-1} or below. For all of the conditions tested, the highest CO yield is measured at 26.7% using the K-promoted WC catalyst at a WHSV 0.28 mL g^{-1} s^{-1}, corresponding to roughly 89% of the equilibrium limited value at 350 °C.[21]

Finally, to characterize the stability of the WC catalysts, the *"H_2 treated"* samples were tested at 350 °C, under the conditions described in Table 3 for a total of 120 hours. Product selectivity remained constant over the entirety of the experiment, but CO_2 conversion decreases slightly with time. Figure 8 plots the CO yields recorded for the three catalysts over the course of this experiment. Both the unpromoted and K-promoted WC catalysts demonstrate moderate deactivation with time, with CO yields 3.1 and 7.0% lower after 120 hours on stream, respectively. The drop in activity for these two systems appears to be greatest during the initial 52 hours on stream, with the rate of deactivation decreasing for both catalysts as a function of time on stream. Interestingly, the Na-promoted WC catalyst demonstrates no observable decrease in CO yield over the entirety of the experiment. For the unpromoted and K-promoted WC catalysts, the decrease in catalytic activity over the course of this experiment is on the order of a previous report for Mo_2C catalysts.[38] This is notable, since the current experiments are at temperatures 50 °C higher than those reported for Mo_2C. Overall, the supported WC-based catalysts are active, selective and stable for the low temperature RWGS reaction.

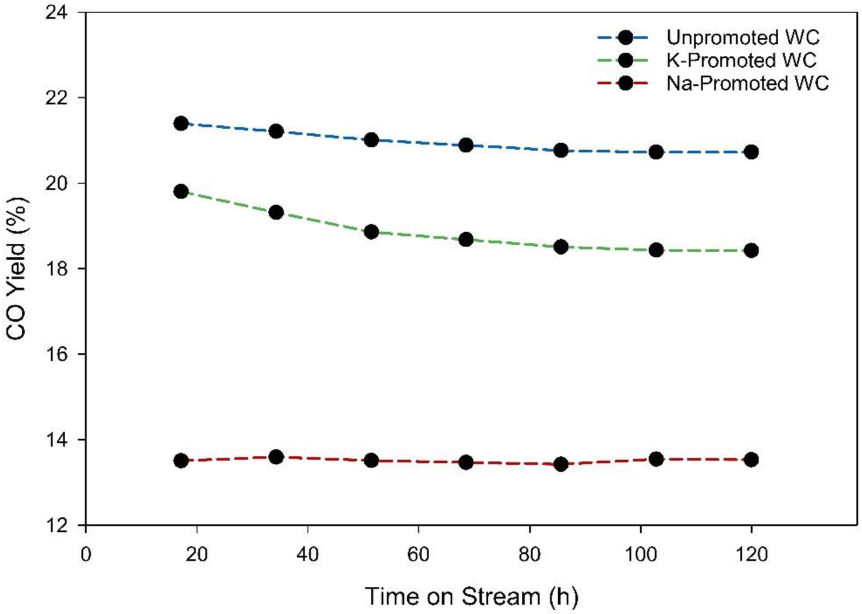

Figure 8: CO yield versus time on stream for "H_2 treated" unpromoted (blue), Na-promoted (red), and K-promoted (green) WC/γ-Al_2O_3. Catalysts were tested at 350 °C using a WHSV of 1.01 mL g^{-1} s^{-1} and a 3:1 H_2:CO_2 ratio at a total pressure of 2.0 MPa.

5.0 Conclusions:

We have established that both Na and K promoters improve the selectivity of WC for the RWGS reaction at low temperatures (300-350 °C), although their presence reduces the overall CO_2 conversions, with Na having more of an inhibiting effect than K. For all WC samples, significant improvement in catalytic performance is realized upon treatment of the catalysts under H_2 at 750 °C, which removes polymeric carbon that is deposited during TPC of the catalyst precursors. W_2C/γ-Al_2O_3 and W/γ-Al_2O_3 were also tested for the RWGS reaction, and found to be active, but less effective than the WC phase. The CO_2 conversion for the K-promoted WC catalyst was comparable to the unpromoted WC catalyst under identical conditions, and provided the highest CO yield of 26.7% at 350 °C. The effects of the alkali metal promoters have been well characterized with several analytical techniques, which demonstrate the WC catalyst exhibits both structural and electronic modification upon the introduction of Na and K species. This work demonstrates the efficacy of WC/γ-Al_2O_3 as a low temperature, RWGS catalyst, and further establishes the role of alkali promoters as a means to tune catalyst selectivity.

6.0 References

(1) Coffey, T.; Hardy, D.; Besencruch, G.; Schultz, K.; Brown, L.; Dahlburg, J. Hydrogen as a Fuel for DOD. *Def. Horizons* **2003**, *36*, 1-11.

(2) Dorner, R.; Hardy, D.; Williams, F. Influence of Gas Feed Composition and Pressure on the Catalytic Conversion of CO2 to Hydrocarbons Using a Traditional Cobalt-Based Fischer- Tropsch Catalyst. *Energy & Fuels* **2009**, *23*, 4190–4195. https://doi.org/10.1021/ef900275m.

(3) Willauer, H. D.; Hardy, D. R.; Lewis, M. K.; Ndubizu, E. C.; Williams, F. W. Effects of Pressure on

the Recovery of CO2 by Phase Transition from a Seawater System by Means of Multilayer Gas Permeable Membranes. *J. Phys. Chem. A* **2010**, *114*, 4003–4008. https://doi.org/10.1021/jp910603f.

(4) Willauer, H. D.; Dimascio, F.; Hardy, D. R.; Williams, F. W. Feasibility of CO2 Extraction from Seawater and Simultaneous Hydrogen Gas Generation Using a Novel and Robust Electrolytic Cation Exchange Module Based on Continuous Electrodeionization Technology. *Ind. Eng. Chem. Res.* **2014**, *53*, 12192–12200. https://doi.org/10.1021/ie502128x.

(5) Willauer, H. D.; DiMascio, F.; Hardy, D. R.; Lewis, M. K.; Williams, F. W. Development of an Electrochemical Acidification Cell for the Recovery of CO2 and H2 from Seawater. *Ind. Eng. Chem. Res.* **2011**, *50*, 9876–9882. https://doi.org/10.1021/ie2008136.

(6) Willauer, H. D.; Dimascio, F.; Hardy, D. R.; Lewis, M. K.; Williams, F. W. Development of an Electrochemical Acidification Cell for the Recovery of CO2 and H2 from Seawater II. Evaluation of the Cell by Natural Seawater. *Ind. Eng. Chem. Res.* **2012**, *51* (34), 11254–11260. https://doi.org/10.1021/ie301006y.

(7) Willauer, H. D.; DiMascio, F.; Hardy, D. R.; Williams, F. W. Development of an Electrolytic Cation Exchange Module for the Simultaneous Extraction of Carbon Dioxide and Hydrogen Gas from Natural Seawater. *Energy & Fuels* **2017**, 31, 1723-1730. https://doi.org/10.1021/acs.energyfuels.6b02586.

(8) Willauer, H. D.; Hardy, D. R.; Lewis, M. K.; Ndubizu, E. C.; Williams, F. W. Extraction of CO2 from Seawater and Aqueous Bicarbonate Systems by Ion-Exchange Resin Processes. *Energy and Fuels* **2010**, *24*, 6682–6688. https://doi.org/10.1021/ef101212e.

(9) DiMascio, F.; Hardy, D.; Lewis, K.; Willauer, H.; Williams, F. Extraction of Carbon Dioxide and Hydrogen From Seawater and Hydrocarbon Production Therefrom. US 2016/0215403 A1.

(10) Willauer, H. D.; Hardy, D. R.; Schultz, K. R.; Williams, F. W. The Feasibility and Current Estimated Capital Costs of Producing Jet Fuel at Sea Using Carbon Dioxide and Hydrogen. *J. Renew. Sustain. Energy* **2012**, *4*, 033111. https://doi.org/10.1063/1.4719723.

(11) Dorner, R. W.; Hardy, D. R.; Williams, F. W.; Willauer, H. D. K and Mn Doped Iron-Based CO2 Hydrogenation Catalysts: Detection of KAlH4 as Part of the Catalyst's Active Phase. *Appl. Catal. A Gen.* **2010**, *373*, 112–121. https://doi.org/10.1016/j.apcata.2009.11.005.

(12) Dorner, R. W.; Hardy, D. R.; Williams, F. W.; Willauer, H. D. C_2-C_{5+} Olefin Production from CO2 Hydrogenation Using Ceria Modified Fe/Mn/K Catalysts. *Catal. Commun.* **2011**, *15*, 88–92. https://doi.org/10.1016/j.catcom.2011.08.017.

(13) Drab, D. M.; Willauer, H. D.; Olsen, M. T.; Ananth, R.; Mushrush, G. W.; Baldwin, J. W.; Hardy, D. R.; Williams, F. W. Hydrocarbon Synthesis from Carbon Dioxide and Hydrogen: A Two-Step Process. *Energy & Fuels* **2013**, *27*, 6348–6354. https://doi.org/10.1021/ef4011115.

(14) Willauer, H. D.; Ananth, R.; Olsen, M. T.; Drab, D. M.; Hardy, D. R.; Williams, F. W. Modeling and Kinetic Analysis of CO2 Hydrogenation Using a Mn and K-Promoted Fe Catalyst in a Fixed-Bed Reactor. *J. CO2 Util.* **2013**, *3–4*, 56–64. https://doi.org/10.1016/j.jcou.2013.10.003.

(15) Bradly, M.J.; Ananth, R.; Willauer, H. D.; Baldwin, J.W.; Hardy, D.R.; Dimascio, F.; Williams, F.W. The Role of Catalyst Environment on CO2 Hydrogenation in a Fixed Bed Reactor. J. CO2 Util. 2017, 17, 1-9. https://doi.org/10.1016/j.jcou.2016.10.014.

(16) Wang, W.; Wang, S.; Ma, X.; Gong, J. Recent Advances in Catalytic Hydrogenation of Carbon Dioxide. *Chem. Soc. Rev.* **2011**, *40*, 3703. https://doi.org/10.1039/c1cs15008a.

(17) Prieto, G. Carbon Dioxide Hydrogenation into Higher Hydrocarbons and Oxygenates: Thermodynamic and Kinetic Bounds and Progress with Heterogeneous and Homogeneous Catalysis. *ChemSusChem* **2017**, *10*, 1056–1070. https://doi.org/10.1002/cssc.201601591.

(18) Ma, Z.; Porosoff, M. D. Development of Tandem Catalysts for CO2 Hydrogenation to Olefins. *ACS Catal.* **2019**, *9*, 2639–2656. https://doi.org/10.1021/acscatal.8b05060.

(19) Porosoff, M. D.; Yan, B.; Chen, J. G. Catalytic Reduction of CO2 by H2 for Synthesis of CO, Methanol and Hydrocarbons: Challenges and Opportunities. *Energy Environ. Sci.* **2016**, *9*, 62-73. https://doi.org/10.1039/C5EE02657A.

(20) Riedel, T.; Claeys, M.; Schulz, H.; Schaub, G.; Nam, S.; Jun, K.; Choi, M.; Kishan, G.; Lee, K. Comparative Study of Fischer–Tropsch Synthesis with H2/CO and H2/CO2 Syngas Using Fe and Co-based Catalysts, *Appl. Catal A Gen*. **1999**, *186*, 201–213. https://doi.org/10.1109/TPEL.2014.2321562.

(21) Riedel, T.; Schaub, G.; Jun, K.-W.; Lee, K.-W. Kinetics of CO2 Hydrogenation on a K-Promoted Fe Catalyst. *Ind. Eng. Chem. Res.* **2001**, *40*, 1355–1363. https://doi.org/10.1021/ie000084k.

(22) Daza, Y.; Kuhn, J. N. CO2 Conversion by Reverse Water Gas Shift Catalysis: Comparison of Catalysts and Mechanisms and Their Consequences for CO2 Conversion to Liquid Fuels. *RSC Adv.* **2016**, *6*, 49675–49691. https://doi.org/10.1039/C6RA05414E.

(23) Daza, Y. A.; Kent, R. A.; Yung, M. M.; Kuhn, J. N. Carbon Dioxide Conversion by Reverse Water-Gas Shift Chemical Looping on Perovskite-Type Oxides. *Ind. Eng. Chem. Res.* **2014**, *53*, 5828–5837. https://doi.org/10.1021/ie5002185.

(24) Chen, C. S.; Cheng, W. H.; Lin, S. S. Study of Iron-Promoted Cu/SiO2 Catalyst on High Temperature Reverse Water Gas Shift Reaction. *Appl. Catal. A Gen.* **2004**, *257*, 97–106. https://doi.org/10.1016/S0926-860X(03)00637-9.

(25) Chen, C. S.; Cheng, W. H.; Lin, S. S. Enhanced Activity and Stability of a Cu/SiO2 Catalyst for the Reverse Water Gas Shift Reaction by an Iron Promoter. *Chem. Commun.* **2001**, *1*, 1770–1771. https://doi.org/10.1039/b104279n.

(26) Su, X.; Yang, X.; Zhao, B.; Huang, Y. Designing of Highly Selective and High-Temperature Endurable RWGS Heterogeneous Catalysts: Recent Advances and the Future Directions. *J. Energy Chem.* **2017**, *26*, 854–867. https://doi.org/10.1016/j.jechem.2017.07.006.

(27) Xie, C.; Chen, C.; Yu, Y.; Su, J.; Li, Y.; Somorjai, G. A.; Yang, P. Tandem Catalysis for CO2 Hydrogenation to C2–C4 Hydrocarbons. *Nano Lett.* **2017**, *17*, 3798–3802. https://doi.org/10.1021/acs.nanolett.7b01139.

(28) Chen, X.; Su, X.; Duan, H.; Liang, B.; Huang, Y.; Zhang, T. Catalytic Performance of the Pt/TiO2 Catalysts in Reverse Water Gas Shift Reaction: Controlled Product Selectivity and a Mechanism Study. *Catal. Today* **2017**, *281*, 312–318. https://doi.org/10.1016/j.cattod.2016.03.020.

(29) Goguet, A.; Meunier, F. C.; Tibiletti, D.; Breen, J. P.; Burch, R. Spectrokinetic Investigation of Reverse Water-Gas-Shift Reaction Intermediates over a Pt/CeO2 catalyst. *J. Phys. Chem. B* **2004**, *108*, 20240–20246. https://doi.org/10.1021/jp047242w.

(30) Porosoff, M. D.; Chen, J. G. Trends in the Catalytic Reduction of CO2 by Hydrogen over Supported Monometallic and Bimetallic Catalysts. *J. Catal.* **2013**, *301*, 30–37. https://doi.org/10.1016/j.jcat.2013.01.022.

(31) Levy, R. B.; Boudart, M. Platinum-like Behavior of Tungsten Carbide in Surface Catalysis. *Science* **1973**, *181* (4099), 547–549. https://doi.org/10.1126/science.181.4099.547.

(32) *The Chemistry of Transtion Metal Carbides and Nitrides*, First ed.; Ted Oyama, S., Ed.; Blackie Academic and Professional: New York.

(33) Chen, J. G. Carbide and Nitride Overlayers on Early Transition Metal Surfaces: Preparation, Characterization, and Reactivities. *Chem. Rev.* **1996**, *96*, 1477–1498. https://doi.org/10.1021/cr950232u.

(34) Porosoff, M. D.; Kattel, S.; Li, W.; Liu, P.; Chen, J. G. Identifying Trends and Descriptors for Selective CO2 Conversion to CO over Transition Metal Carbides. *Chem. Commun.* **2015**, *51*, 6988–6991. https://doi.org/10.1039/C5CC01545F.

(35) Dorner, R. W.; Hardy, D. R.; Williams, F. W.; Willauer, H. D. Heterogeneous Catalytic CO2 Conversion to Value-Added Hydrocarbons. *Energy Environ. Sci.* **2010**, *3*, 884–890. https://doi.org/10.1039/C001514H.

(36) Gnanamani, M. K.; Hamdeh, H. H.; Shafer, W. D.; Hopps, S. D.; Davis, B. H. Hydrogenation of Carbon Dioxide over Iron Carbide Prepared from Alkali Metal Promoted Iron Oxalate. *Appl. Catal. A Gen.* **2018**, *564*, 243–249. https://doi.org/10.1016/j.apcata.2018.07.034.

(37) Woo, H. C.; Park, K. Y.; Kim, Y. G.; Namau]Jong ShikChung, I. S.; Lee, J. S. Mixed Alcohol Synthesis from Carbon Monoxide and Dihydrogen over Potassium-Promoted Molybdenum Carbide Catalysts. *Appl. Catal.* **1991**, *75*, 267–280. https://doi.org/10.1016/S0166-9834(00)83136-X.

(38) Porosoff, M. D.; Baldwin, J. W.; Peng, X.; Mpourmpakis, G.; Willauer, H. D. Potassium-Promoted Molybdenum Carbide as a Highly Active and Selective Catalyst for CO2 Conversion to CO. *ChemSusChem* **2017**, *10*, 2408–2415. https://doi.org/10.1002/cssc.201700412.

(39) Sullivan, M. M.; Chen, C. J.; Bhan, A. Catalytic Deoxygenation on Transition Metal Carbide Catalysts. *Catal. Sci. Technol.* **2016**, *6*, 602–616. https://doi.org/10.1039/c5cy01665g.

(40) Ramanathan, S.; Oyama, S. T. New Catalysts for Hydroprocessing: Transition Metal Carbides and Nitrides. *J. Phys. Chem.* **1995**, *99*, 16365–16372. https://doi.org/10.1021/j100044a025.

(41) Dubois, J.-L.; Sayama, K.; Arakawa, H. CO2 Hydrogenation Over Carbide Catalysts. *Chem. Lett.* **1992**, *21*, 1992.

(42) Wu, S. Y.; Ho, J. J. Adsorption, Dissociation, and Hydrogenation of CO2 on WC(0001) and WC-Co Alloy Surfaces Investigated with Theoretical Calculations. *J. Phys. Chem. C* **2012**, *116*, 13202–13209. https://doi.org/10.1021/jp302901r.

(43) Ledoux, M. J.; Huu, C. P.; Guille, J.; Dunlop, H. Compared Activities of Platinum and High Specific Surface Area Mo2C and WC Catalysts for Reforming Reactions. I. Catalyst Activation and Stabilization: Reaction of n-Hexane. *J. Catal.* **1992**, *134*, 383–398. https://doi.org/10.1016/0021-9517(92)90329-G.

(44) Oyama, S. T. Preparation and Catalytic Properties of Transition Metal Carbides and Nitrides.

Catal. Today **1992**, *15*, 179–200. https://doi.org/10.1016/0920-5861(92)80175-M.

(45) Claridge, J. B.; York, A. P. E.; Brungs, A. J.; Marquez-alvarez, C.; Sloan, J.; Tsang, S. C.; Green, M. L. H. New Catalysts for the Conversion of Methane to Synthesis Gas : Molybdenum and Tungsten Carbide. *J. Catal.* **1998**, *100*, 85–100. https://doi.org/10.1006/jcat.1998.2260.

(46) Ribeiro, F. H.; Betta, R. A. D.; Guskey, G. J.; Boudart, M. Preparation and Surface Composition of Tungsten Carbide Powders with High Specific Surface Area. *Chem. Mater.* **1991**, 9, 805–812. https://doi.org/10.1021/cm00017a015.

(47) Xiao, T.; York, A. P. E.; Coleman, K. S.; Claridge, J. B.; Sloan, J.; Charnock, J.; Green, M. L. H. Effect of Carburising Agent on the Structure of Molybdenum Carbides. *J. Mater. Chem.* **2001**, *11*, 3094–3098. https://doi.org/10.1039/b104011c.

(48) Volpe, L.; Boudart, M. Compounds of Molybdenum and Tungsten with High Specific Surface Area. II. Carbides. *J. Solid State Chem.* **1985**, *59*, 348–356. https://doi.org/10.1016/0022-4596(85)90301-9.

(49) Giraudon, J.; Devassine, P.; Lamonier, J.; Delannoy, L.; Leclercq, L.; Leclercq, G. Synthesis of Tungsten Carbides by Temperature-Programmed Reaction with CH4 / H2 Mixtures . Influence of the CH4 and Hydrogen Content in the Carburizing Mixture. **2000**, *426*, 412–426. https://doi.org/10.1006/jssc.2000.8859.

(50) Löfberg, A.; Frennet, A.; Leclercq, G.; Leclercq, L.; Giraudon, J. M. Mechanism of WO3 Reduction and Carburization in CH4/H2 Mixtures Leading to Bulk Tungsten Carbide Powder Catalysts. *J. Catal.* **2000**, *189*, 170–183. https://doi.org/10.1006/jcat.1999.2692.

(51) Leclercq, G.; Kamal, M.; Giraudon, J. M.; Devassine, P.; Feigenbaum, L.; Leclercq, L.; Frennet, A.; Bastin, J. M.; Löfberg, A.; Decker, S. Study of the Preparation of Bulk Powder Tungsten Carbides by Temperature Programmed Reaction with CH4+ H2 mixtures. *J. Catal.* **1996**, *158*, 142–169. https://doi.org/10.1006/jcat.1996.0015.

(52) Dirck Vermaire, P. V. B. The Preparation of WO3/TiO2 and WO3/Al2O3 and Characterization Reduction. *J. Catal.* **1989**, *116*, 309–317.

(53) Feng, L.; Li, X.; Dadyburjor, D. B.; Kugler, E. L. A Temperature-Programmed-Reduction Study on Alkali-Promoted, Carbon-Supported Molybdenum Catalysts. *J. Catal.* **2000**, *190*, 1–13. https://doi.org/10.1006/jcat.1999.2744.

(54) Chappell, P. J. C.; Kibel, M. H.; Baker, B. G. X-Ray Photoelectron and Ion Scattering Studies of Tungsten Oxides and Tungsten Oxide Catalysts. *J. Catal.* **1988**, *110*, 139–149. https://doi.org/10.1016/0021-9517(88)90304-1.

(55) Yang, Y.; Xiang, H.; Xu, Y.; Bai, L.; Li, Y. Effect of Potassium Promoter on Precipitated Iron-Manganese Catalyst for Fischer – Tropsch Synthesis. **2004**, *266*, 181–194. https://doi.org/10.1016/j.apcata.2004.02.018.

(56) Li, S.; Li, A.; Krishnamoorthy, S.; Iglesia, E. Effects of Zn, Cu, and K Promoters on the Structure and on the Reduction, Carburization, and Catalytic Behavior of Iron-Based Fischer-Tropsch Synthesis Catalysts. *Catal. Letters* **2001**, *77*, 197–205. https://doi.org/10.1023/A:1013284217689.

(57) Pimenta, M. T. B.; Apr, A.; Curvelo, S.; Teixeira, V. Physical and Chemical Studies of Tungsten Carbide Catalysts : Effects of Ni Promotion and Sulphonated Carbon. **2015**, 5, 23874–23885.

https://doi.org/10.1039/c5ra03252k.

(58) Hara, Y.; Minami, N.; Itagaki, H. Synthesis and Characterization of High-Surface Area Tungsten Carbides and Application to Electrocatalytic Hydrogen Oxidation. **2007**, *323*, 86–93. https://doi.org/10.1016/j.apcata.2007.02.011.

(59) Ribeiro, F.; Boudart, M.; Dalla Betta, R.; Iglesia, E. Catalytic Reactions of N-Alkanes on Beta-W2C and WC: The Effect of Surface Oxygen on Reaction Pathways. *J. Catal.* **1991**, *130*, 498–513. https://doi.org/10.1016/0021-9517(91)90131-M.

(60) Yang, X.; Kimmel, Y. C.; Fu, J.; Koel, B. E.; Chen, J. G. Activation of Tungsten Carbide Catalysts by Use of an Oxygen Plasma Pretreatment. *ACS Catal.* **2012**, *2*, 765–769. https://doi.org/10.1021/cs300081t.

(61) Kimmel, Y. C.; Esposito, D. V; Birkmire, R. W.; Chen, J. G. Effect of Surface Carbon on the Hydrogen Evolution Reactivity of Tungsten Carbide (WC) and Pt-Modified WC Electrocatalysts. *Int. J. Hydrogen Energy* **2011**, *37*, 3019–3024. https://doi.org/10.1016/j.ijhydene.2011.11.079.

(62) Leclercq, G.; Kamal, M.; Lamonier, J.; Feigenbaum, L.; Malfoy, P.; Leclercq, L. Treatment of Bulk Group VI Transition Metal Carbides with Hydrogen and Oxygen. **1995**, *121*, 169–190.

(63) Choi, P. H.; Jun, K.; Lee, S.; Choi, M.; Lee, K. Hydrogenation of Carbon Dioxide over Alumina Supported Fe-K Catalysts. **1996**, *40*, 115–118.

(64) Meiri, N.; Dinburg, Y.; Amoyal, M.; Koukouliev, V.; Nehemya, R. V.; Landau, M. V.; Herskowitz, M. Novel Process and Catalytic Materials for Converting CO2 and H2 Containing Mixtures to Liquid Fuels and Chemicals. *Faraday Discuss.* **2015**, *183*, 197–215. https://doi.org/10.1039/C5FD00039D.

(65) Saeidi, S.; Amin, N. A. S.; Rahimpour, M. R. Hydrogenation of CO2 to Value-Added Products - A Review and Potential Future Developments. *J. CO2 Util.* **2014**, *5*, 66–81. https://doi.org/10.1016/j.jcou.2013.12.005.

(66) Li, J.; Cheng, X.; Zhang, C.; Chang, Q.; Wang, J.; Wang, X. Applied Catalysis A : General Effect of Alkalis on Iron-Based Fischer-Tropsch Synthesis Catalysts : Alkali-FeOx Interaction , Reduction , and Catalytic Performance. *Applied Catal. A, Gen.* **2016**, *528*, 131–141. https://doi.org/10.1016/j.apcata.2016.10.006.

(67) Moulder, J.; Stickle, W.; Sobol, P.; Bomben, K. *Handbook of X-Ray Photoelectron Spectroscopy*; Chastain, J., Ed.; Perkin Elmer: Minnesota, 1992.

(68) Xiang, M.; Li, D.; Zou, J.; Li, W.; Sun, Y.; She, X. XPS Study of Potassium-Promoted Molybdenum Carbides for Mixed Alcohols Synthesis via CO Hydrogenation. *J. Nat. Gas Chem.* **2010**, *19*, 151–155. https://doi.org/10.1016/S1003-9953(09)60051-7.

(69) Amoyal, M.; Vidruk-Nehemya, R.; Landau, M. V.; Herskowitz, M. Effect of Potassium on the Active Phases of Fe Catalysts for Carbon Dioxide Conversion to Liquid Fuels through Hydrogenation. *J. Catal.* **2017**, *348*, 29–39. https://doi.org/10.1016/j.jcat.2017.01.020.

(70) Park, J. C.; Yeo, S. C.; Chun, D. H.; Lim, J. T.; Yang, J. Il; Lee, H. T.; Hong, S.; Lee, H. M.; Kim, C. S.; Jung, H. Highly Activated K-Doped Iron Carbide Nanocatalysts Designed by Computational Simulation for Fischer-Tropsch Synthesis. *J. Mater. Chem. A* **2014**, *2*, 14371–14379. https://doi.org/10.1039/c4ta02413c.

(71) Wu, Q.; Christensen, J. M.; Luca, G.; Duchstein, L. D. L.; Wagner, J. B.; Temel, B.; Grunwaldt, J.; Jensen, A. D. Supported Molybdenum Carbide for Higher Alcohol Synthesis from Syngas. *Catal. Today* **2013**, *215*, 162–168. https://doi.org/10.1016/j.cattod.2013.03.002.

(72) Li, T.; Virginie, M.; Khodakov, A. Y. Effect of Potassium Promotion on the Structure and Performance of Alumina Supported Carburized Molybdenum Catalysts for Fischer-Tropsch Synthesis. *Appl. Catal. A, Gen.* **2017**, *542*, 154–162. https://doi.org/10.1016/j.apcata.2017.05.018.

(73) Dorkis, L.; Rodriguez, J. A.; Koverga, A. A.; Flo, E. CO, CO2, and H2 Interactions with (0001) and (001) Tungsten Carbide Surfaces : Importance of Carbon and Metal Sites. *J. Phys. Chem. C* **2019**, 123, 8871-8883. https://doi.org/10.1021/acs.jpcc.8b11840.

(74) Dixit, M.; Peng, X.; Porosoff, M. D.; Willauer, H. D.; Mpourmpakis, G. Elucidating the Role of Oxygen Coverage in CO2 Reduction on Mo2C. *Catal. Sci. Technol.* **2017**, *7*, 5521–5529. https://doi.org/10.1039/c7cy01810j.